Capillarity

Vol. 19, No. 2, p. 39-47, 2026

Original article

# Measurements of copper droplet oscillations on tungsten substrate and the angular dependence of the oscillation frequency

Sergei Zhevnenko*, Mikhail Slinkin

*Physical Chemistry Department, National University of Science and Technology MISIS, Moscow 119049, Russia*

**Keywords:**
Copper melt
tungsten
high-speed imaging
droplet oscillations
contact angle

**Cited as:**
Zhevnenko, S., Slinkin, M. Measurements of copper droplet oscillations on tungsten substrate and the angular dependence of the oscillation frequency. Capillarity, 2026, 19(2): 39-47.
https://doi.org/10.46690/capi.2026.05.01

**Abstract:**
The study of droplet impingement and subsequent oscillations on solid substrates is critical for understanding wetting dynamics and heat transfer in applications such as spray cooling and metal coating. However, existing experimental approaches often rely on low-speed imaging or manual analysis, which limits their ability to capture rapid, transient oscillations and achieve high precision, particularly under extreme high-temperature and vacuum conditions. Moreover, conventional methods face challenges in automatically extracting key dynamic parameters like contact spot diameter and oscillation frequencies without user intervention. Novel methods for the computer processing of high-speed video images from experiments on droplet impingement and subsequent oscillations on a solid substrate were developed and validated. The image analysis algorithms, implemented in the Python programming language utilizing the OpenCV computer vision library, enable automated, high-precision tracking of dynamic droplet parameters. These methods were successfully applied to real high-temperature experiments involving molten copper droplets falling onto a polished tungsten substrate under vacuum conditions. Through automated image processing, time-dependent evolutions of the droplet center-of-mass coordinates, the diameter of the contact spot with the solid surface, and the dynamic contact wetting angles for the Cu/W system were obtained. The analysis reveals that upon impact, the droplet undergoes damped shape oscillations. The fundamental oscillation frequencies of the droplets and their dependence on mass were determined with high accuracy. Furthermore, by integrating data from other experimental systems, a generalized angular dependence of the oscillation frequency for sessile droplets was established and compared with existing theoretical models.

## 1. Introduction

Accurate measurement of liquid properties like viscosity and surface tension is crucial for numerous industrial and scientific applications, particularly when sample volumes are minimal (Sun et al., 2003). Oscillating droplets present a promising method for extracting these properties, as their resonant frequencies and damping characteristics are intrinsically linked to surface tension and viscous dissipation, respectively (Strani and Sabetta, 1984; Yao et al., 2017; Dai et al., 2018). While the foundational theory for free, levitated drops was established by Rayleigh (1879) and Chandrasekhar (1959), translating this to sessile droplets on flat substrates introduces significant complexity due to solid-liquid interactions. This

Yandy Scientific Press

*Corresponding author.
*E-mail address*: zhevnenko@misis.ru (S. Zhevnenko); slinkin.misha2311@gmail.com (M. Slinkin).


Received March 13, 2026; revised April 6, 2026; accepted April 28, 2026; available online May 2, 2026.

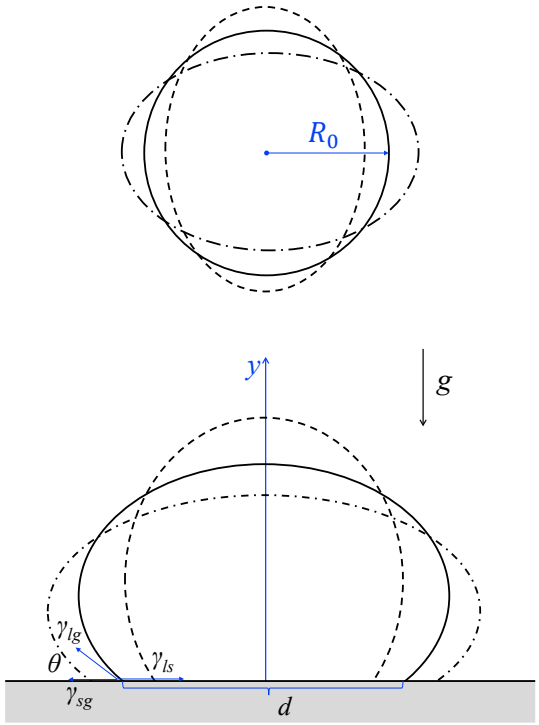


**Fig. 1**. Schematic diagram of the change in shape of a small droplet with radius $R_0$ when it falls on a solid substrate. $\theta$ is the contact angle, $d$ is the contact diameter. $\gamma_{sg}$, $\gamma_{ls}$, $\gamma_{lg}$ are surface tensions of solid-gas, liquid-solid and liquid-gas interface, respectively, $g$ is gravity.

has spurred extensive experimental work, driven by diverse applications ranging from spray cooling and inkjet printing to enhanced mixing (Castrejon-Pita et al., 2013), collection of suspended particles (Whitehill et al., 2010), drop shedding (Qi et al., 2010), and the actuation of droplet motion on functional surfaces (Daniel et al., 2001; Wright and Saylor, 2003; Shilton et al., 2008).

Experimental investigations have employed various methods to excite and monitor droplet oscillations (Egry et al., 2005): An acoustic levitation technique (Tian et al., 1997), by vibrating orifice droplet generator (Brenn and Frohn, 1993), impulse gas flow (Sharp, 2012), by ultrasonic surface acoustic waves (Brunet et al., 2010). Motion detection leverages high-speed imaging, optical deflection techniques, and position-sensitive detectors. Such studies have been pivotal for applications like electric-field-enhanced extraction, electrospray synthesis, and measuring contact angles in complex fluids. Crucially, they have revealed that the solid substrate fundamentally alters the droplet's resonant behavior compared to a levitated state, introducing contact-line dynamics and additional damping mechanisms.

The resonant dynamics of a sessile droplet are governed by key parameters: The equilibrium contact angle ($\theta$), the gravitational Bond number (Bo), and the mobility of the three-phase contact line, as it demonstrated at Fig. 1. The contact line condition (whether pinned or freely moving) is particularly critical, as it defines the energy dissipation at the solid boundary and splits the classical Rayleigh-Lamb spectrum (Sakakeeny and Ling, 2021). Although inviscid theories for both limits exist, and the pinned moving contact line case has received considerable experimental validation, a comprehensive understanding of the freely moving contact line regime (highly relevant for superhydrophobic and liquid-infused surfaces) remains incomplete (Amberg, 2022). Moreover, while factors influencing damping such as bulk viscosity, boundary layers, and moving contact lines have been qualitatively discussed, a detailed theoretical and experimental study of how viscosity and contact angle jointly govern energy dissipation in sessile drops is still lacking (Yasuri, 2025).

When a droplet falls onto a solid surface, equilibrium is not reached immediately. Under the influence of gravity, the droplet tends to spread across the surface – the contact area between the droplet and the surface increases, the center of mass lowers, and the contact angle changes. At the same time, surface tension forces cause the droplet to "retract", i.e., decrease the drop area, which again alters the droplet's parameters. Thus, damped oscillations of the droplet's shape are observed, the degree of damping depending on the viscosity of the liquid, adhesion, and other factors. The droplet parameters observed during its oscillations are called dynamic parameters. The droplet parameters observed after it reaches equilibrium are called equilibrium parameters. This equilibrium is described by Young's equation (Young, 1805; Dupré, 1869):

$$\gamma_{sg} = \gamma_{ls} + \gamma_{lg}\cos\theta \tag{1}$$

where $\gamma_{sg}$ is the surface tension of solid-gas interface, N/m; $\gamma_{ls}$ is the surface tension of liquid-solid interface, N/m; $\gamma_{lg}$ is the surface tension of liquid-gas interface, N/m; $\theta$ is the contact angle in equilibrium state, °.

Good wetting corresponds to an angle $\theta_0$ value from 0° to 90°, while an angle $\theta_0$ from 90° to 180° is referred to as non-wetting or hydrophobicity.

Drop oscillation methods involve analyzing the oscillation frequencies of a drop and then calculating its surface tension. One approach to measuring the frequencies of an oscillating drop is to hold it in an electromagnetic field, the so-called levitated drop method. A similar method was used in (Harrison et al., 1977; Soda et al., 1978; Kasama et al., 1980) to determine the surface tension of copper. Another approach involves determining the frequencies of a drop in free fall (Brillo et al., 2005; Fahimi et al., 2023). The oscillation frequencies of a freely falling or levitating drop are related to the surface tension through the equation (Rayleigh, 1879; Chandrasekhar, 1959):

$$\omega_k = \sqrt{\frac{k(k-1)(k+2)\gamma_{lg}}{3\pi m}} \tag{2}$$

where $k$ is a natural number indicating the mode of oscillation. For $k = 2$:

$$\omega_2^2 = \frac{8\gamma_{lg}}{3\pi m} \tag{3}$$

where $\omega$ is the second mode oscillation frequency, $Hz^2$; $m$ is the droplet mass, kg.

The damping coefficient of the droplet oscillations is determined by its viscosity, as shown in the work (Lamb, 1932).

The damping coefficient Γ depends on the viscosity $\eta$, Pa·s; the radius of the droplet $R_0$ and its mass $m$:

$$\Gamma = \frac{20\pi\eta R_0}{3m} \tag{4}$$

The oscillation dynamics of liquid drops differ fundamentally depending on whether the drop is free (e.g., levitated or in microgravity) or sessile (adhering to a solid substrate). Free drops (e.g., in levitation) are ideally spherical and force-free, described by Rayleigh's theory for inviscid oscillations. The boundary conditions are governed by surface tension and inertia. Sessile drops are constrained by a solid support, breaking spherical symmetry. The contact line (where liquid, solid, and gas meet) introduces additional boundary conditions: Pinned (fixed contact line), natural (fixed contact angle), or dynamic (contact angle depends on contact-line speed).

Free drops exhibit degenerate oscillation modes described by spherical harmonics. Sessile drops show split spectra due to substrate interaction. In sessile drops, contact-line motion (pinned, mobile, or dynamically wetting) significantly affects oscillation frequencies and damping. Free drops assume a spherical shape; deviations (e.g., due to levitation fields) are treated as perturbations. Sessile drops adopt spherical-cap shapes parameterized by contact angle. Free drops do not exhibit such substrate-driven instabilities; however, they may experience rotational or translational mode splitting in presence of external fields. Free drops are modeled using Rayleigh–Lamb theory, extended to include viscosity, external fields, and sample rotation. Sessile drops require solutions to Laplace's equation in spherical-cap coordinates, with eigenvalue problems incorporating contact-line conditions via inverse operator methods or Rayleigh–Ritz variational techniques (Egry et al., 2005; Bostwick and Steen, 2014).

While both free and sessile drops exhibit capillary-driven oscillations, the presence of a solid substrate in sessile drops introduces complex dynamics due to contact-line constraints, breaking of spectral degeneracy, and additional dissipation mechanisms. Understanding these differences is crucial for applications in microfluidics, coating processes, and precision measurement techniques.

The resonant frequency of sessile liquid droplets can be calculated by using a theory that was originally developed by Noblin et al. (2004). This model assumes that under conditions of resonant vibration, the profile length ($l$) of the droplet will contain a half integer number of wavelengths ($\lambda$), such that:

$$l = 2R\theta = \frac{n\lambda}{2} \tag{5}$$

where $R$ is the radius of curvature of the droplet, $\theta$ is the three phase contact angle and $n$ is an integer corresponding to the mode number ($n = 2,\ 3,\ 4$). In this and all subsequent equations, the angle $\theta$ is given in radians. Under the influence of small amplitude vibrations, the three phase contact line is assumed to remain fixed during vibration and as such is expected to coincide with the position of nodes in the excited waveform.

The volume, $V$, of a small droplet can be used to determine its radius of curvature if its shape is approximated to that of a spherical cap such that:

$$V = \frac{m}{\rho} = \frac{\pi R^3}{3}\left(\cos^3\theta - 3\cos\theta + 2\right) \tag{6}$$

where $m$ is the mass of the droplet and $\rho$ is density. The spherical cap approximation used in deriving the above equation is only valid when the radius of curvature is smaller than the capillary length (Sharp et al., 2011), i.e., when $R < L_{cap} = (\gamma_g/\rho g)^{1/2}$, $g$ is the acceleration due to gravity. In this regime, surface tension is expected to dominate over the influence of gravity which acts to flatten the profile of the droplet and to form a puddle. For metallic drops with about 1 N/m surface tension and 10,000 kg/m$^3$ density, $R$ should be less than 3 mm. All studied drops in our experiment do not exceed 2 mm in radius.

An expression for the contact angle dependence of the frequencies of the vibrational modes of sessile droplets is (Sharp et al., 2011):

$$\omega_n = \frac{\alpha\pi}{2}\sqrt{\frac{n^3\gamma_{lg}\left(\cos^3\theta - 3\cos\theta + 2\right)}{24m\theta^3}} \tag{7}$$

Sharp et al. (2011) performed detailed measurements of the contact angle dependence of the resonant frequency of sessile water droplets and found that Eq. (7) worked well and that values of $\alpha = 0.81$ and $n = 2$ could be used to accurately predict the frequencies of the lowest vibrational mode in sessile droplets with contact angles in the range $12^\circ \sim 160^\circ$. Both, Eqs. (2) and (7) predicts a linear scaling between the square of the resonant frequency and the reciprocal of the droplet mass.

Most prior experimental studies have been limited to a narrow range of contact angles or single-surface systems at near-room temperatures, leaving a significant gap in the systematic exploration of the contact-angle dependence of resonant frequencies and, especially, damping. This work aims to provide experimental investigation into the oscillation of sessile droplets on flat surfaces at high temperatures, with a focused analysis on the effects of contact angle, substrate interaction, and the associated damping mechanisms that are paramount for practical applications.

## 2. Experimental

The wetting and infiltration experiments were conducted using the setup illustrated in Fig. 2 and described in detail in (Zhevnenko et al., 2021; Protsenko et al., 2023). The substrates were placed on a movable lower stage, while the melt's dispenser was positioned in a heater above the substrate. A vacuum of $10^{-3}$ Pa was maintained throughout the experiment using a combination of rotary and diffusion pumps. The experiments on drop falling were performed at various temperatures ranging from 1,100 to 1,250 °C. The infiltration process was recorded using a high-speed SSD CP70-2-M/C-1000 camera and an infrared Optris PI 1M cameras.

The substrate was cut from coarse-grained, annealed pure tungsten, ground, and polished. Copper and gallium do not form intermetallic compounds with tungsten, and the solubility of tungsten in copper is extremely low (Subramanian and Laughlin, 1991). Data on the density of liquid copper were

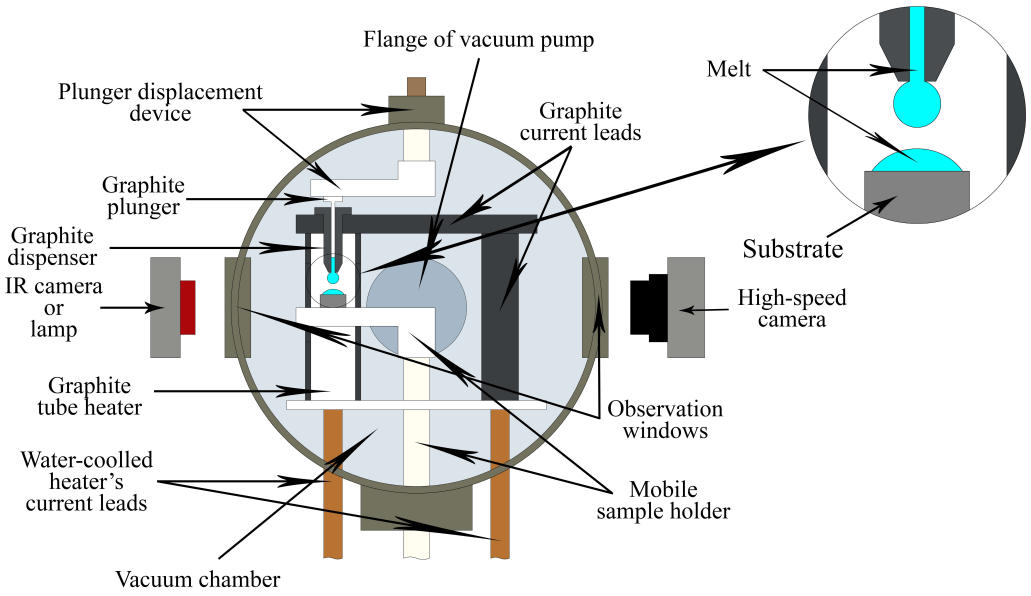


**Fig. 2**. Schematic of the experimental setup designed for direct measurements of wetting and infiltration.

taken from Assael et al. (2010).

## 2.1 Method for determining the droplet's center of mass

The determination of the droplet's center of mass was performed by calculating the spatial moments of the contour extracted from the image. This method allows for the quantitative characterization of intensity distribution within the extracted region. However, in this case, pixel intensities do not contribute to the moment values, as the method processes binarized images where the intensities of pixels belonging to the droplet are uniform. Thus, by considering the droplet as homogeneous, i.e., with uniformly distributed mass throughout its volume, the calculation of the center of mass coordinates is reduced to finding the arithmetic mean of the droplet's pixel coordinates along the X and Y axes.

To determine the coordinates of the droplet's center of mass, the cv2.moments function was used, which calculates the moments of the region outlined by the contour. These moments are then utilized to compute the center of mass coordinates according to the formulas:

$$\begin{cases} C_x = \dfrac{m_{10}}{m_{00}} \\ C_y = \dfrac{m_{01}}{m_{00}} \end{cases} \tag{8}$$

where $C_x$ and $C_y$ are the coordinates of the droplet's center of mass along the X and Y axes, respectively; $m_{10}$ and $m_{01}$ are the first-order spatial moments, reflecting the total distribution of coordinates in the horizontal and vertical directions, respectively; $m_{00}$ is the zeroth-order moment, which, in the case of a binary image, equals the number of pixels belonging to the object.

This method for determining the droplet's center of mass is characterized by its accuracy, robustness, and ease of implementation. The center of mass calculated from moments accurately reflects the distribution of "mass" (pixels) within the extracted contour, which is particularly important when analyzing droplet dynamics. The method performs well even with minor variations in object shape.

## 2.2 Method for estimating droplet volume

Let us represent a droplet in an image as a series of consecutive pixel rows. Suppose the width of each row, i.e., the number of pixels in each row, corresponds to the base diameter of a cylinder with a height of one pixel. Assuming that at any given moment the droplet can be approximated as a solid of revolution, its volume can be estimated using the formula:

$$V_{drop} = \sum_{i=1}^{n} V_i = \sum_{i=1}^{n} h_i \frac{\pi}{4} d_i^2 \tag{9}$$

where $V_{drop}$ is the drop's volume; $V_i$ is the volume of the $i$-th cylinder; $h_i$ is the height of the $i$-th cylinder, equal to one pixel; $d_i$ is the diameter of the cylinder's base, i.e., the number of pixels in the $i$-th row.

## 2.3 Method for determining contact angles

Once the extreme contact points between the droplet and the surface were identified, it became possible to determine the contact angles. To achieve this, a method for constructing a tangent to the droplet surface at these extreme contact points with the substrate was required. A linear approximation, or least squares method, was employed for this purpose. In the vicinity of each contact point, several consecutive points along the droplet contour were selected (the optimal number of such points depends on the image resolution; in this case, with a resolution of 256 by 160 pixels, it was set by default to seven). Using the NumPy library, these points were subjected to linear regression via the least squares method. This procedure yields

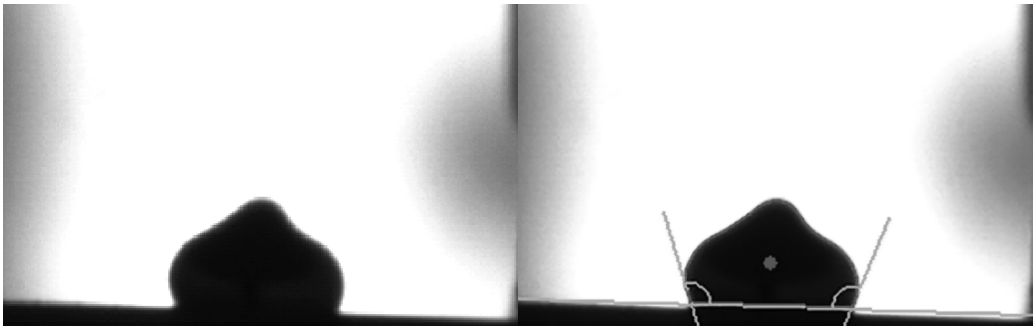

**Fig. 3**. An example of the original and processed frame with a sessile drop.

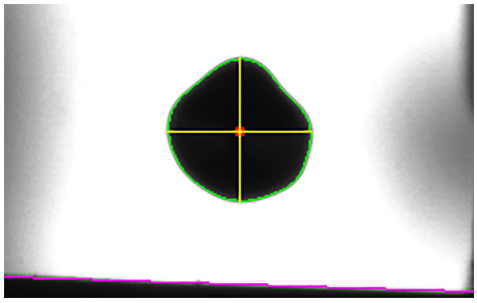

**Fig. 4**. An example of a processed frame with a drop in free fall.

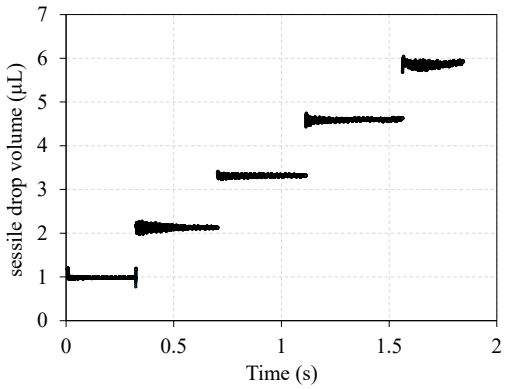


**Fig. 5**. Automatically estimated volume of a sessile drop, increasing as it merges with other falling drops for copper on tungsten at 1,125 °C.

the slope of the tangent to the droplet surface at its extreme contact point.

However, this slope is calculated relative to the horizontal axis of the frame. Therefore, it is necessary to account for the inclination of the line representing the upper boundary of the substrate. Consequently, the apparent contact angle is calculated based on the slopes of the tangent line and the substrate line.

A special case was considered separately, when the tangent slope was 90° relative to the frame's horizontal. This scenario was defined by conditions where either the points selected for tangent analysis were vertically aligned, or where the tangent slope was exceedingly large. In such instances, the linear approximation method becomes inapplicable, and the 90° slope is assigned manually. An example of the original and processed images, visualizing the droplet contour, center of mass, and contact angles, is presented in Fig. 3.

### *2.4 Vertical and horizontal diameters of a free falling droplet*

For droplets in the free-fall phase, the vertical and horizontal diameters are calculated. The horizontal diameter is defined as the distance between the two farthest contour points located on the horizontal line passing through the center of mass. Similarly, the vertical diameter is calculated as the distance between the uppermost and lowermost points lying on the vertical line also passing through the droplet's center of mass.

Since the calculation is performed for droplets in free fall, it is necessary to establish a condition for identifying this state. Obviously, the free-fall phase concludes when the droplet begins to interact with the substrate, i.e., makes contact with it. To verify this condition, an analysis of the contour points' proximity to a defined baseline corresponding to the surface is used. Upon detection of contact, the diameter calculation is not performed. Fig. 4 presents an example of a processed image of a droplet in the free-fall period.

## 3. Results and discussion

In the experiments, the falling of copper and copper-gallium melt droplets onto a tungsten surface was observed using high-speed imaging at a rate of 15,000-20,000 $s^{-1}$. Upon impact, the droplet oscillates: The contact angles, contact spot diameter, and center of mass change periodically. The experiments involved varying the temperature, the volume of the oscillating droplet, and its composition (which influences the wetting contact angle, surface tension, and melt density).

As an example, the results of an experiment on the falling of copper melt droplets at a temperature of 1,125 °C onto a polished tungsten substrate, analyzed using the aforementioned algorithms, are provided. The volume of each droplet was calculated as the average of the volumes determined in each frame containing the corresponding droplet. The time dependencies of the calculated droplet volumes are shown in Fig. 5. As can be seen from the figure, oscillations of five droplets with sequentially increasing volume were recorded during a single experiment.

Oscillations of the contact diameter (Fig. 6), the coordinates of the center of mass (Fig. 7(a)), and the contact angles (Fig. 7(b)) can be effectively determined simultaneously with

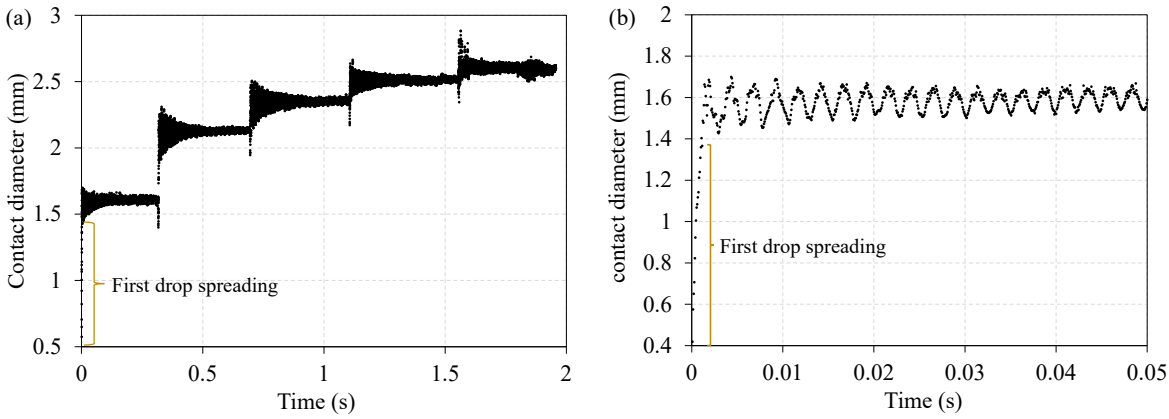


**Fig. 6**. (a) Time dependence of the contact diameter of Cu melt on W and (b) contact diameter the oscillating first drop. It is marked the spreading period for first drop.

**Table 1**. Drop's parameters for pure copper on tungsten at 1,125 °C and for Cu+5at.%Ga on tungsten at 1,280 °C.

| Type | Drop's number (-) | Sessile drop volume ($mm^3$) | Drop's weight ($kg \cdot 10^{-6}$) | Frequency of the lowest mode (Hz) |
|---|---|---|---|---|
| Pure Cu | 1 | 1.02 | 8.1 | 411 |
| | 2 | 2.18 | 17.3 | 300 |
| | 3 | 3.37 | 26.8 | 239 |
| | 4 | 4.66 | 37.0 | 203 |
| | 5 | 5.96 | 47.3 | 178 |
| Cu+5 at.%Ga | 1 | 1.18 | 9.2 | 399 |
| | 2 | 3.25 | 25.4 | 261 |
| | 3 | 6.30 | 49.1 | 173 |

the parameters characterizing the spreading process (the spreading rate and the dynamic wetting angle). Fig. 7 clearly shows a decrease in the oscillation frequency as the droplet size increases due to coalescence. The experiment was conducted on a Cu+5 at.% Ga melt in vacuum at a temperature of 1,280 °C.

The dependence of the fundamental mode oscillation frequency on the size of the copper droplet on a solid substrate is shown in Fig. 8. The frequency data are included in the Table 1.

The contact angles near which droplet oscillations occur are quite close for copper and copper with gallium, ranging from 80° to 90°. According to Silze et al. (2016), surface tension is virtually independent of gallium content up to 10 at.% Ga in molten copper. The temperature dependence of surface tension is also small. Thus, the dependence of the square of the droplet oscillation frequency on the reciprocal mass, as follows from Eq. (7), should be linear and virtually identical for both melts. Fig. 9 demonstrates this. A linear approximation through the origin was constructed using the least-squares method. The linear coefficient was found to be approximately 1.49 for Cu+5at.%Ga melt and 1.42 for pure copper.

Meanwhile, there is an extreme relationship between the contact angle and the oscillation frequency of the droplet on the substrate, as follows from Eq. (7). Data was collected from other systems studied previously, and plotted the angular dependence of the oscillation frequency as the product of the square of the frequency and the contact angle (Fig. 10). It can be seen from the graph that the frequencies for drops with angles of about 90o do not correspond to the dependence for the main oscillation mode ($n = 2$). This is the region of angles with the minimum inertial component (the smallest mass must be displaced for the oscillation process to occur). It is likely that several oscillation modes are realized simultaneously during oscillations in this region of angles. The deviation observed near 90° (Fig. 10) suggests that the oscillation dynamics in this angular range may be more complex than captured by the simple $n = 2$ mode model. One possible explanation is the simultaneous excitation of multiple oscillation modes. This hypothesis is supported by theoretical work (Bostwick and Steen, 2014) showing that eigenfrequencies for different modes can approach each other near certain contact angles, potentially leading to mode coupling. Spectral analysis of our centroid motion data (presented in Supplementary Material) provides preliminary evidence of multiple frequency components for droplets with $\theta \approx 90°$, while droplets with significantly different angles show predominantly single-frequency behavior. However, we acknowledge that definitive proof would require more sophisticated modal analysis techniques, which we identify as an important direction for future research.

For the droplets in our study, the radius of curvature $R$ was consistently below 2 mm, which is less than the capillary length for copper ($\sim$ 5 mm), validating the spherical cap approximation used in Eqs. (6) and (7). However, examination of Fig. 6 reveals that the contact line is not strictly pinned du-ring oscillations, the contact diameter varies periodically. The droplet diameter changes, but not significantly. At the same time, high-temperature experiments are characterized by the pinning of the contact line due to the rapid formation of surface morphology (a depression under the melt).

The deviation observed near 90° (Fig. 10) suggests that the oscillation dynamics in this angular range may be more com-

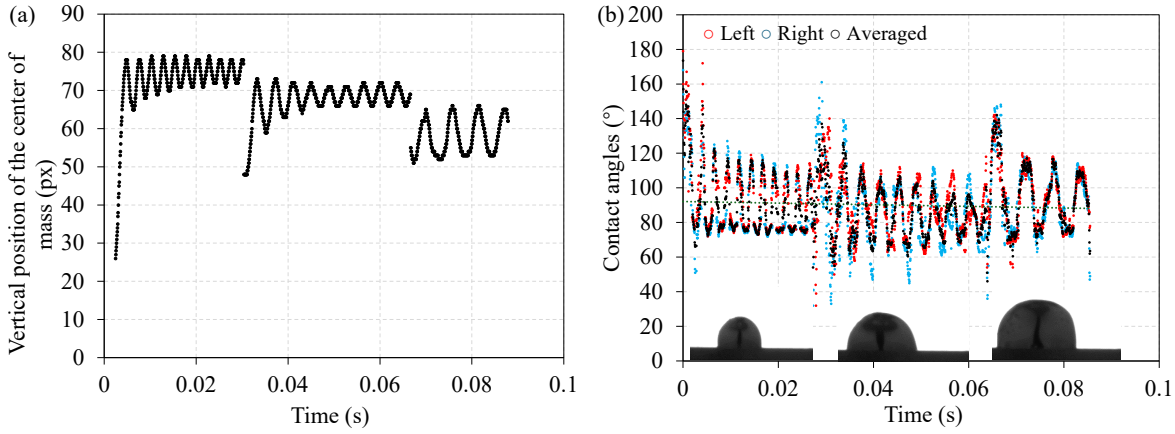


**Fig. 7**. (a) Time dependence of the mass center of a sessile drop and (b) increasing as it merges with other falling drops for Cu+5Ga on tungsten at 1,280 °C.

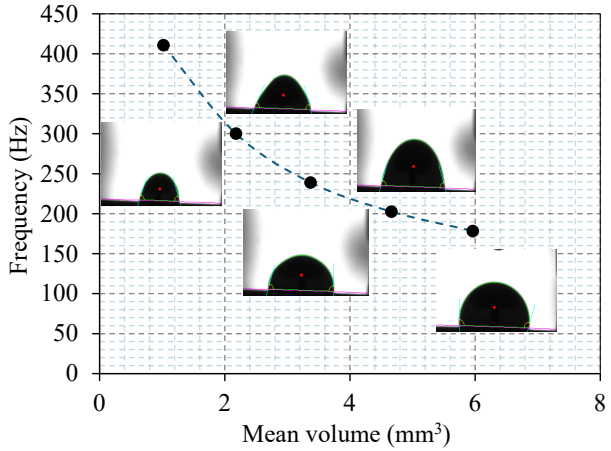


**Fig. 8**. Dependence of the frequency of droplet oscillations on the volume for Cu on W at 1,125 °C.

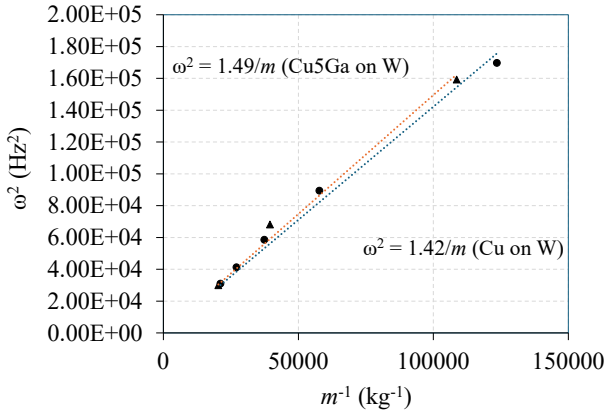


**Fig. 9**. Dependence of the square of the frequency of the lowest frequency oscillations on the inverse mass.

plex than captured by the simple $n = 2$ mode model. This finding implies that the relationship between contact angle and resonant frequency is not monotonic, but rather exhibits a local extremum where the inertial resistance to shape change is minimized. One plausible explanation for the elevated frequencies near 90° is the simultaneous excitation of multiple oscillation modes. This hypothesis is supported by theoretical work (Bostwick and Steen, 2014) showing that eigenfrequencies for different modes can approach each other near certain contact angles, potentially leading to mode coupling and spectral splitting. However, a critical observation from our experiments complicates this picture: The contact line is not strictly pinned during oscillations—the contact diameter varies periodically (Fig. 6). This mobility contradicts the fixed-contact-line assumption underlying Eq. (7) and suggests that the true boundary condition lies between the pinned and freely moving limits. In high-temperature metallic systems, this behavior may be further complicated by the rapid formation of surface morphology (a depression under the melt), which can induce localized pinning and alter the effective restoring forces. Therefore, while the simple $n = 2$ model captures the overall mass scaling, the detailed frequency behavior – particularly near 90°-likely reflects a convolution of multiple factors: Mode coupling, contact-line dynamics, and temperature-dependent interfacial restructuring.

The data compiled in Fig. 10 originate from different experimental systems with varying temperatures, compositions, and substrate materials. The alpha coefficient is set to 1.15. The surface tension is assumed to be 1.3 J/m$^2$, $n = 2$. While this introduces some uncertainty in direct quantitative comparison, the frequency data was normalized by the factor $\alpha \cdot (\gamma/m)1/2$ to account for differences in surface tension and mass. Nevertheless, differences in contact line mobility, substrate roughness, and chemical interactions could influence the oscillation frequencies independent of contact angle. The systematic deviation near 90° observed across multiple systems suggests a genuine physical phenomenon rather than experimental artifacts, but more controlled studies with systematic variation of individual parameters are needed to confirm this interpretation. The transition from a free to a sessile configuration fundamentally alters the oscillation spectrum in several ways. First, the spherical symmetry of free drops is broken by the presence of the substrate, lifting the degeneracy of oscillation modes described by spherical harmonics. For a free drop, the mode with degree $l = 2$ has five independent eigenmodes with identical frequencies ($2l + 1$ degeneracy). In contrast, a sessile drop on a flat substrate exhibits mode spli-

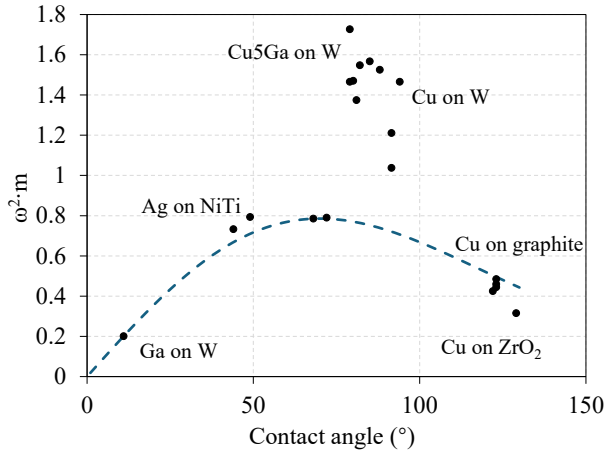


**Fig. 10**. Angular dependence of the oscillation frequency of a melt droplet on the surface of a solid substrate. The dotted line corresponds to the theoretical dependence.

tting, with different eigenfrequencies for axisymmetric and non-axisymmetric oscillations (Bostwick and Steen, 2014). Second, the contact line introduces new boundary conditions that constrain the admissible velocity fields. Third, additional dissipation mechanisms emerge from contact line friction and viscous boundary layers near the solid surface. Fourth, the equilibrium shape is no longer spherical but a spherical cap, altering the restoring force distribution. These modifications collectively result in a frequency spectrum that depends strongly on contact angle and contact line mobility, as captured (though incompletely) by Eq. (7). Our experimental data, particularly the deviation from Eq. (7) near 90°, suggests that the actual spectral modifications may be even more complex than current theoretical models predict, potentially involving mode interactions that are absent in free drops.

## 4. Conclusions

This experimental study investigated the complex dynamics of molten metal droplet impingement and subsequent oscillations on a solid tungsten substrate at high temperatures. The primary outcomes and contributions of the work are summarized as follows:

1) A robust computational methodology was developed and implemented for the automated analysis of high-speed video recordings. Utilizing Python and the OpenCV library, the algorithms provide reliable, high-throughput extraction of key dynamic parameters: Droplet center-of-mass trajectory, contact diameter, contact angles, and volume. This method represents a significant tool for studying fast wetting and oscillation phenomena in high-temperature systems.
2) The oscillation dynamics of sessile copper droplets were quantitatively characterized. A clear inverse relationship between the fundamental oscillation frequency and droplet mass (and volume) was experimentally confirmed, aligning with the theoretical scaling of $\omega^2 \propto 1/m$. The linear dependence of $\omega^2$ on the inverse mass was demonstrated for both pure Cu and Cu-5at.%Ga melts, with closely matched coefficients ($\sim 1.42$ and $\sim 1.49$, respectively). This indicates that, within the studied composition range, the primary physical properties governing oscillation frequency (surface tension, density) remain largely unaffected by the addition of gallium, consistent with literature data.
3) The role of the contact angle was examined. While the mass dependence followed theoretical predictions for a given angle, the analysis of a broader dataset revealed a significant deviation from the simple model for contact angles near 90°. The observed frequencies in this angular region were higher than predicted for the fundamental mode ($n = 2$), suggesting a more complex dynamical regime. This may indicate the simultaneous excitation of multiple oscillation modes or a shift in the dominant dissipation mechanism when the contact angle approaches 90°, where the inertial component of the oscillation is minimized.

## Acknowledgements

The research was carried out with the support of the Ministry of Science and Higher Education of the Russian Federation within the framework of the State Assignment FSME-2023-0007.

## Conflicts of interest

The authors declare no competing interest.



## References

Adam, N. K. Use of the term 'Young's Equation' for contact angles. Nature, 1957, 180(4590): 809-810.

Amberg, G. Detailed modelling of contact line motion in oscillatory wetting. npj Microgravity, 2022, 8: 1.

Assael, M. J., Kalyva, A. E., Antoniadis, K. D., et al. Reference data for the density and viscosity of liquid copper and liquid tin. Journal of Physical and Chemical Reference Data, 2010, 39(3): 033105.

Barsoum, M. W., Radovic, M. Elastic and mechanical properties of the MAX phases. Annual Review of Materials Research, 2011, 41: 195-227.

Bostwick, J. B., Steen, P. H. Dynamics of sessile drops. Part 1. Inviscid theory. Journal of Fluid Mechanics, 2014, 760: 5-38.

Brenn, G., Frohn, A. An experimental method for the investigation of droplet oscillations in a gaseous medium. Experiments in Fluids, 1993, 15(2): 85-90.

Brillo, J., Egry, I. Surface tension of nickel, copper, iron and their binary alloys. Journal of Materials Science, 2005, 40(8): 2213-2216.

Brunet, P., Baudoin, M., Bou Matar, O., et al. Droplet displacements and oscillations induced by ultrasonic surface acoustic waves: A quantitative study. Physical Review E, 2010, 81(3): 036315.

Castrejon-Pita, J. R., Baxter, W. R. S., Morgan, J., et al. Fu-

ture, opportunities and challenges of inkjet technologies. Atomization and Sprays, 2013, 23(6): 541-565.

Chandrasekhar, S. On the stability of a spinning liquid drop. Proceedings of the London Mathematical Society, 1959, 3(9): 141-149.

Dai, X., Sun, N., Nielsen, S. O., et al. Hydrophilic directional slippery rough surfaces for water harvesting. Science Advances, 2018, 4: eaaq0919.

Daniel, S., Chaudhury, M. K., Chen, J. C. Fast drop movements resulting from the phase change on a gradient surface. Science, 2001, 291(5504): 633-636.

Dupré, A. Thermodynamic theory. Paris, France, Gauthier-Villars, 1869. (in French)

Egry, I., Giffard, H., Schneider, S. The oscillating drop technique revisited. Measurement Science and Technology, 2005, 16(2): 426-431.

Fahimi, K., Mädler, L., Ellendt, N. Measurement of surface tension with free-falling oscillating molten metal droplets: A numerical and experimental investigation. Experiments in Fluids, 2023, 64: 133.

Harrison, D. A., Yan, D., Blairs, S. The surface tension of liquid copper. Journal of Chemical Thermodynamics, 1977, 9: 1111-1119.

Ji, S., Gu, Q., Xia, B. Porosity dependence of mechanical properties of solid materials. Journal of Materials Science, 2006, 41: 1757-1768.

Kasama, A., McLean, A., Miller, W. A. Temperature dependence of the surface tension of liquid copper. Canadian Metallurgical Quarterly, 1980, 19(4): 399-401.

Lamb, H. Hydrodynamics. Cambridge, United Kingdom, Cambridge University Press, 1932.

Li, S., Yu, W., Zhai, H., et al. Mechanical properties of low-temperature synthesized dense and fine-grained $Cr_2AlC$ ceramics. Journal of the European Ceramic Society, 2011, 31(1-2): 217-224.

Noblin, X., Buguin, A., Brochard-Wyart, F. Vibrations of sessile drops. European Physical Journal E, 2004, 14: 395-404.

Pittoni, P. G., Chang, Y., Lin, S. The effect of interfacial morphology on wetting of graphite by molten silver at high temperature. Journal of Materials Science, 2012, 47: 8395-8403.

Protsenko, P. V., Gorshenkov, M. V., Zhevnenko, S. N., et al. Wetting and spreading of Pb, Pb-Cu, and Ag-Cu melts on a polycrystalline copper surface with cobalt particles. Journal of Alloys and Compounds, 2023, 948: 169785.

Qi, A., Yeo, L., Friend, J., Ho, J. The extraction of liquid, protein molecules and yeast cells from paper through surface acoustic wave atomization. Lab on a Chip, 2010, 10: 470-476.

Rayleigh, R. W. S. On the capillary phenomena of jets. Proceedings of the Royal Society of London, 1879, 29: 71-97.

Sakakeeny, J., Ling, Y. Numerical study of natural oscillations of supported drops with free and pinned contact lines. Physics of Fluids, 2021, 33(6): 062109.

Sarina, B. A. O., Tang, K., Kvithyld, A., et al. Wetting of pure aluminium on graphite, SiC, and $Al_2O_3$ in aluminium filtration. Transactions of Nonferrous Metals Society of China, 2012, 22(8): 1930-1938.

Sharp, J. S. Resonant properties of sessile droplets; contact angle dependence of the resonant frequency and width in glycerol/water mixtures. Soft Matter, 2012, 8(2): 399-407.

Sharp, J. S., Farmer, D. J., Kelly, J. Contact angle dependence of the resonant frequency of sessile water droplets. Langmuir, 2011, 27: 9367-9371.

Shilton, R., Tan, M. K., Yeo, L. Y., et al. Particle concentration and mixing in microdrops driven by focused surface acoustic waves. Journal of Applied Physics, 2008, 104(1): 014910.

Silze, F., Wiehl, G., Kaban, I., et al. Wetting behaviour of Cu-Ga alloys on 304L steel. Materials & Design, 2016, 91: 11-18.

Soda, H., McLean, A., Miller, W. A. Surface tension measurements of liquid copper droplets in the temperature range 1000 to 1330°C. Transactions of the Japan Institute of Metals, 1978, 18: 614-619.

Strani, M., Sabetta, F. Free vibrations of a drop in partial contact with a solid support. Journal of Fluid Mechanics, 1984, 141: 233-247.

Subramanian, P. R., Laughlin, D. E. Cu-W (Copper-tungsten). In: Phase Diagrams of Binary Tungsten Alloys, 1991: 76-79.

Sun, S., Zhang, L., Jahanshahi, S. From viscosity and surface tension to Marangoni flow in melts. Metallurgical and Materials Transactions B, 2003, 34(5): 517-523.

Tian, Y., Holt, R. G., Apfel, R. E. Investigation of liquid surface rheology of surfactant solutions by droplet shape oscillations: Experiments. Journal of Colloid and Interface Science, 1997, 187(1): 1-10.

Whitehill, J., Neild, A., Ng, T. W., et al. Collection of suspended particles in a drop using low frequency vibration. Applied Physics Letters, 2010, 96(5): 053501.

Wright, P. H., Saylor, J. R. Patterning of particulate films using Faraday waves. Review of Scientific Instruments, 2003, 74(9): 4063-4070.

Yao, C.-W., Lai, C.-L., Alvarado, J. L., et al. Experimental study on effect of surface vibration on micro textured surfaces with hydrophobic and hydrophilic materials. Applied Surface Science, 2017, 412: 45-51.

Yasuri, K. A. Energy dissipation mechanisms in droplet dynamics: Implications for wetting phenomena. Microfluidics and Nanofluidics, 2025, 29(11): 71.

Young, T. An essay on the cohesion of fluids. Philosophical Transactions of the Royal Society of London, 1805, 95: 65-87.

Zhevnenko, S., Gorshenkov, M., Petrov, I. Effect of B on improving wetting and imbibition of sintered porous Ta by Cu melt. Journal of Alloys and Compounds, 2021, 860: 157886.